



## Temperature dependence of charge transport in single-layer graphene on surface-terminated diamond

Aisuloo Aitkulova <sup>ID</sup>\*, Markus Gabrysch <sup>ID</sup>, Saman Majdi <sup>ID</sup>, Nattakarn Suntornwipat <sup>ID</sup>, Jan Isberg <sup>ID</sup>

Department of Electrical Engineering, Uppsala University, Box 65, Uppsala, 751 03, Sweden

### ARTICLE INFO

#### Keywords:

Diamond  
Graphene  
Surface termination  
Hall effect

### ABSTRACT

The integration of single-layer graphene with diamond substrates offers a promising platform for high-performance electronic devices by utilizing the exceptional properties of both materials. This study describes a fabrication process and transport measurements of single-layer graphene devices on diamond substrates featuring two surface terminations: hydrogen (H-terminated, thermal process) and oxygen (O-terminated, plasma treatment). The carrier transport properties were investigated using Hall effect measurements over a broad temperature range (80–400 K) under high-vacuum conditions ( $1 \times 10^{-4}$  mbar). Our findings reveal that thermal annealing significantly improves the graphene-diamond interface quality, causing a notable increase in carrier mobility for devices on both H- and O-terminated from 1439 to 1644  $\text{cm}^2/\text{Vs}$  and from 1238 to 1340  $\text{cm}^2/\text{Vs}$ , respectively. We also found that the effect of remote interfacial phonon scattering on high-temperature mobility is affected by the termination type. These findings highlight the importance of substrate surface engineering and offer a pathway for optimizing graphene-diamond heterostructures for advanced electronic applications.

### 1. Introduction

Over the past few years, interest in diamond-based technologies has surged, driven by discoveries of nitrogen-vacancy (NV) center applications [1]. Besides its applications in quantum technologies and heat management [2], diamond is also appealing for electronic applications [3]. To achieve comparable levels of development in electronic applications, additional methodological approaches are necessary. These include doping, surface functionalization, heterostructure fabrication, and scaling up diamond synthesis.

Another carbon allotrope, graphene — a two-dimensional material distinguished by its exceptional mechanical strength, outstanding optical transparency, and high charge-carrier mobility — has attracted considerable scientific interest due to its potential for diverse advanced technological applications. These include high-performance electronics [4], photonic devices [5], neuromorphic computing systems [6], and quantum computing platforms [7], as well as emerging platforms for twistrionics and straintrionics [8,9]. Despite its advantageous properties, integrating graphene into complementary metal–oxide–semiconductor (CMOS) technology remains a substantial challenge. This difficulty primarily arises from the lack of well-defined, scalable “process units” for graphene-based device fabrication and modification, as well as the complex interface interactions between graphene and other structure layers,

which can adversely affect device performance and process reproducibility [10,11]. Additionally, the growing interest in more sustainable devices and reducing electronic waste is driving the development of all-carbon devices [12].

The integration of graphene with diamond substrates can result in significant enhancements in device performance. Specifically, diamond substrates are crucial for developing high-power and high-frequency all-carbon electronic devices. This necessity stems from diamond's superior ability to manage self-heating, resulting in an enhanced current-carrying capacity exceeding  $10^9$  A/cm<sup>2</sup> [13], alongside markedly improved GFET performance and scaling behavior [14]. Only a few studies have covered the fabrication process and characterization of graphene-based electronic devices on diamond [15].

Therefore, it is essential to develop a reproducible process flow for fabricating basic 2D materials and diamond-based devices. Beyond common steps like wet cleaning, metal deposition, and lithography, it is relatively straightforward to find correlations between device characteristics and process parameters, such as surface termination and annealing. Surface termination is a step in the fabrication process that modifies surface chemistry and directly affects the performance of planar devices on diamond. It has been shown that H-termination reduces surface energy compared to O-termination by

\* Corresponding author.

E-mail address: [aisuloo.aitkulova@angstrom.uu.se](mailto:aisuloo.aitkulova@angstrom.uu.se) (A. Aitkulova).

<https://doi.org/10.1016/j.cartre.2025.100598>

Received 16 October 2025; Received in revised form 23 November 2025; Accepted 1 December 2025

Available online 2 December 2025

2667-0569/© 2025 The Authors. Published by Elsevier Ltd. This is an open access article under the CC BY license (<http://creativecommons.org/licenses/by/4.0/>).

17 mJ/m<sup>2</sup> [16]. Depending on process parameters, H-termination generally results in a hydrophobic (contact angle greater than 90°) surface, while O-termination produces a hydrophilic (contact angle less than 90°) surface. For graphene transfer, a hydrophilic surface is preferred to facilitate the process and prevent the formation of high-density wrinkles [17]. Additionally, for NV centers in close proximity to the sample surface, O-termination has been shown to enhance spin coherence [18], while nitrogen-termination improves the charge stability of near-surface NV<sup>-</sup> centers by reducing charge trapping [19]. Moreover, it has been shown that the tri-acid etching process effectively removes disordered carbon and restores the diamond surface's crystalline structure [20]. Annealing is commonly used to remove adsorbed water from the surface and improve device performance. It has been demonstrated that annealing at 400 K can increase carrier mobility in H-terminated diamond by a factor of two [21].

Here, we present results of Hall effect measurements of single-layer graphene Hall bars on diamond. H- and O-termination of diamond was conducted before graphene transfer, followed by post-annealing at 400 K in vacuum.

## 2. Experimental setup

Hall effect measurements were performed under high-vacuum conditions of approximately  $1 \times 10^{-4}$  mbar across a temperature range of 80 to 400 K. The investigated sample is housed in a Janis ST-300 MS cryostat, cooled with liquid nitrogen. Temperature regulation is achieved with a Lakeshore 331S temperature controller. To avoid charging effects due to deep impurities in diamond, a custom-built AC Hall system based on two 7265 DSP Lock-in amplifiers was used for the Hall-effect measurements. A GMW 3470 water-cooled electromagnet generated a static magnetic field of up to 0.5 T, oriented perpendicular to the device's plane. The measurements were automated utilizing a Keithley 7601 switch system.

## 3. Fabrication

CVD graphene “Easy Transfer” was purchased from Graphenea. CVD electronic-grade (100)-diamond from Element Six, and CVD optical-grade (111)-diamond from Diamond Elements Pvt. Ltd. All diamond samples were wet-cleaned by graphite etch (HNO<sub>3</sub> : HClO<sub>4</sub> : H<sub>2</sub>SO<sub>4</sub>) at 200 °C for 40 min [22], followed by standard RCA cleaning steps [23], including RCA-1 (H<sub>2</sub>O : H<sub>2</sub>O<sub>2</sub> : NH<sub>4</sub>OH, ratio 5:1:1), and RCA-2 (H<sub>2</sub>O : H<sub>2</sub>O<sub>2</sub> : HCl, ratio 5:1:1), and finalized by plasma descum. DI (deionized) water is used for all processes. Metallization of all samples consists of 5/25 nm Ti/Au, deposited using an e-beam evaporator with a base pressure of  $10^{-7}$  Torr. Contacts were patterned by optical lithography. All analyzed samples exhibit a smooth surface morphology, characterized by an average surface roughness of less than 5 nm, as determined by AFM scans.

### 3.1. Oxygen-terminated (111)

After graphite etching, the samples were dry-cleaned using plasma descum with low-power oxygen plasma (50 W, 2 min). In the case of the O-terminated (111) sample, metal contacts were fabricated via a lift-off process after depositing Au/Ti (25/5 nm), followed by the transfer of graphene. After the sacrificial layer was removed, a thin layer of Ti (2 nm) was deposited to protect graphene from additional contamination during patterning. Hall bars were patterned using optical lithography, with  $80 \times 340 \mu\text{m}$  dimensions (Fig. 1). Following this, the sample was bonded to the chip holder and measured in the Hall setup before and after annealing at 400 K.

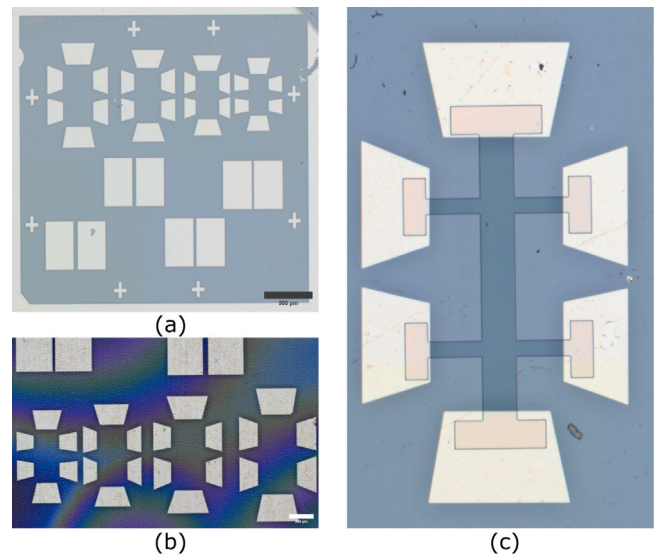


Fig. 1. (a) Sample after contact deposition and patterning before transfer. (b) Sacrificial layer/Graphene after transfer. (c) Graphene Hallbar patterning.

### 3.2. Hydrogen-terminated (100)

After graphite etching, the samples underwent a dry cleaning process utilizing plasma descum with low-power oxygen plasma (50 W, 2 min). Subsequently, after initial sample preparation, hydrogen termination was performed in a furnace, with heating and cooling profiles illustrated in Fig. 2. The sheet resistance was  $220 \text{ k}\Omega/\square$ . H-termination of diamond is well-known to create Negative Electron Affinity (NEA), due to surface transfer doping of the diamond, and a conductive surface, whereas O-termination results in a Positive Electron Affinity (PEA) and a non-conductive surface. Immediately after the hydrogen termination, graphene transfer was executed; for the (100) H-terminated sample, it is critical to note that the transfer was performed before contact fabrication. After transfer, a thin layer of Ti (2 nm) was used as a process shield for graphene. Hall bar structures were patterned using optical lithography. Electrical contacts were formed via a lift-off process following the deposition of Au (25 nm) and Ti (5 nm). The prepared samples were then mounted onto a chip holder and characterized using Hall effect measurements. Following an observation by Yang et al. [21] that mobility increased from 170 to  $340 \text{ cm}^2/\text{V}\cdot\text{s}$  on a H-terminated surface after annealing a sample at 400 K from 170 to  $340 \text{ cm}^2/\text{V}\cdot\text{s}$ , our samples were also annealed at 400 K, and the Hall-effect was measured before and after anneal.

## 4. Results and discussions

We performed Hall effect measurements on graphene hallbars with length and width  $80 \times 340 \mu\text{m}$ , on two diamond samples: O-terminated (111) and H-terminated (100) at different temperature ranges. The measurement temperature ranges with a maximum step of 30 K:

- (1) 80 → 300 K
- (2) 300 → 400 K
- (3) 400 → 80 K

In Fig. 3, the dependence of sheet resistivity and Hall mobility on carrier concentration is plotted for samples with graphene hallbars on O-terminated (111) and H-terminated (100) surfaces, ranging from 80 to 300 K. In the case of O-terminated (111), we observe a higher carrier concentration, but lower Hall mobility, compared to the H-terminated sample (Table 1). For both samples, we observe a decrease in carrier

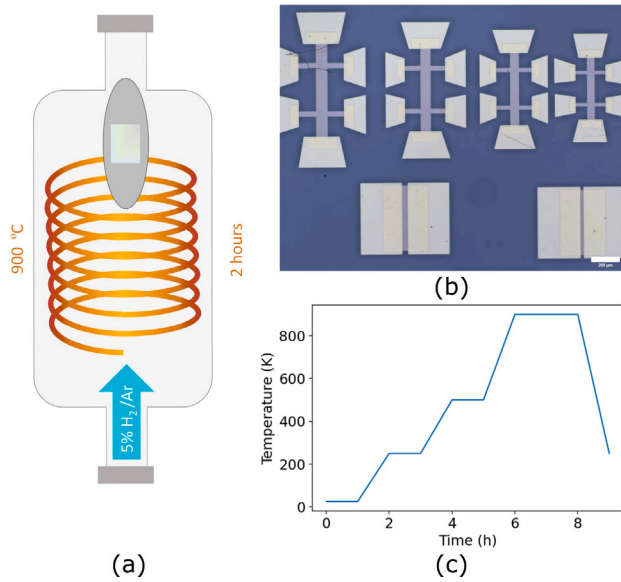


**Fig. 2.** (a) Simplified furnace scheme. (b) Fabrication of  $\text{TiO}_x$  cap on graphene on H-terminated sample. (c) Heating profile during H-termination process.

**Table 1**

Maximum values for mobility  $\mu$ , sheet resistivity  $\rho$  and carrier concentration  $n$  in the interval (80–300) K.

Sample	$n_{\max}$ ( $\text{cm}^{-2}$ )	$\mu_{\max}$ ( $\text{cm}^2/\text{V}\cdot\text{s}$ )	$\rho_{\max}$ ( $\Omega/\square$ )
H-(100)	$4.4 \times 10^{12}$	1439	1045
O-(111)	$6.2 \times 10^{12}$	1238	872

**Table 2**

Maximum values for mobility  $\mu$ , sheet resistivity  $\rho$  and carrier concentration  $n$  in the interval (300–400) K.

Sample	$n_{\max}$ ( $\text{cm}^{-2}$ )	$\mu_{\max}$ ( $\text{cm}^2/\text{V}\cdot\text{s}$ )	$\rho_{\max}$ ( $\Omega/\square$ )
H-(100)	$4.4 \times 10^{12}$	1339	1233
O-(111)	$6 \times 10^{12}$	1171	1076

**Table 3**

Maximum values for mobility  $\mu$ , sheet resistivity  $\rho$  and carrier concentration  $n$  in the interval (400–80) K.

Sample	$n_{\max}$ ( $\text{cm}^{-2}$ )	$\mu_{\max}$ ( $\text{cm}^2/\text{V}\cdot\text{s}$ )	$\rho_{\max}$ ( $\Omega/\square$ )
H-(100)	$2.8 \times 10^{12}$	1644	1597
O-(111)	$4.9 \times 10^{12}$	1340	1198

concentration with increasing temperature, which is due to a shift of the Fermi level relative to the Dirac point. However, for the (111)-sample, we observed a maximum value for carrier concentration at 240 K (Tables 1–2). From 240 to 300 K, the carrier concentration decreases slightly.

In Fig. 4, we observe how the temperature dependencies of Hall resistivity, mobility, and carrier concentration change after annealing at 400 K for 30 min. The annealing step markedly improves the electrical characteristics of both terminations (Table 3).

The pursuit of ultra-high mobility often relies on ideal, small-scale systems—suspended graphene [24] or dry-transferred, hBN-encapsulated exfoliated flakes [25]. These flakes possess pristine intrinsic properties, yet their dimensions are limited to a few micrometres, precluding any scalable technology. In contrast, our devices employ large-area, commercially available CVD graphene. The trade-off of this approach is the polycrystalline nature of the film, which introduces grain-boundary scattering and reduces mobility relative to single-crystal graphene [26]. Within this context, the mobilities reported here

**Table 4**

Values for RIP energy  $E$ , low-temperature mobility  $\mu_l$ , and constant  $c$  by least-squares fits to Hall mobility data in the interval 80–400 K after annealing.

Sample	$E$ (meV)	$\mu_l$ ( $\text{cm}^2/\text{V}\cdot\text{s}$ )	$c \times 10^3$ ( $\text{V}\cdot\text{s}/\text{cm}^2$ )
H-(100)	$114.3 \pm 5.7$	$1641 \pm 2.1$	$-5.5 \pm 0.9$
O-(111)	$60.3 \pm 2.8$	$1341 \pm 2.5$	$-1.2 \pm 0.1$

are comparable to those of previously studied graphene-on-diamond devices [15].

According to theoretical studies [27], with relatively similar binding energies for graphene on H-(100) and O-(111) of  $-50$  and  $-58$  meV, diamond has a minimal effect on graphene. However, there is a possibility of charge transfer between graphene and (111)-diamond. In the case of O-(111), p-doping is possible.

Next, we discuss the temperature dependence of the Hall mobility. It is well known that disorder sources, e.g., impurities and interactions with trapped charges in the substrate, act as scattering centers that affect charge transport in the graphene layer. These scattering sources, along with interface impurities introduced during the transfer process, are the primary sources of impurity scattering. These scattering processes yields a temperature-independent scattering rate [28], and thus a temperature-independent Hall mobility  $\mu_l = \text{const.}$  [29]. In addition to impurity scattering, we include carrier scattering of remote interfacial phonons (RIP), which are caused by optical phonons from the substrate or interfaces [28,30]. Assuming, for simplicity, a single dominant RIP energy  $E$ , the resulting mobility  $\mu_{RIP}$  satisfies:

$$\mu_{RIP} \sim \exp(E/k_B T) - 1 \quad (1)$$

where  $k_B$  is the Boltzmann constant. In combination, these scattering processes yield a total mobility  $\mu$ , by Matthiessen's rule:

$$\frac{1}{\mu} = \frac{1}{\mu_l} + \frac{c}{\exp(E/k_B T) - 1} \quad (2)$$

where  $c$  is a constant. In Fig. 5, we observe how annealing at 400 K improved the interface quality, increasing the low temperature mobility from  $1238 \text{ cm}^2/\text{V}\cdot\text{s}$  to  $1340 \text{ cm}^2/\text{V}\cdot\text{s}$  for the O-terminated sample and from  $1439 \text{ cm}^2/\text{V}\cdot\text{s}$  to  $1644 \text{ cm}^2/\text{V}\cdot\text{s}$  for the H-terminated sample. Using the fitting model (Eq. (2)) with  $\mu_l, E$  and  $c$  as fitting parameters, we obtain a RIP energy of 60 meV (114 meV) for the O-terminated (H-terminated) sample (Table 4). The observed difference in low-temperature mobility can be explained by variations in the impurity concentration in the different substrates and by different interface impurity concentrations between graphene and substrates. Thus, the variation in low-temperature mobility cannot be attributed solely to the choice of termination. However, the observed variation in RIP scattering and its influence on the high-temperature mobility are independent of the substrate impurity concentration. It can be attributed to the choice of termination.

## 5. Summary and conclusions

Single-layer graphene Hallbars ( $80 \times 340 \mu\text{m}$ ) on diamond with H- and O-termination were fabricated and characterized using an AC-Hall setup over a wide temperature range: 80–400 K. Post-anneal measurements revealed a systematic increase of low-temperature mobility for both samples. Annealing at 400 K effectively mitigates transfer-induced defects, thereby enhancing impurity-limited mobility.

In addition, it is shown that the H-terminated sample exhibits a higher energy barrier for remote interfacial scattering. These findings highlight the potential of tailored surface terminations and thermal treatments to enhance the performance of graphene-on-diamond devices.

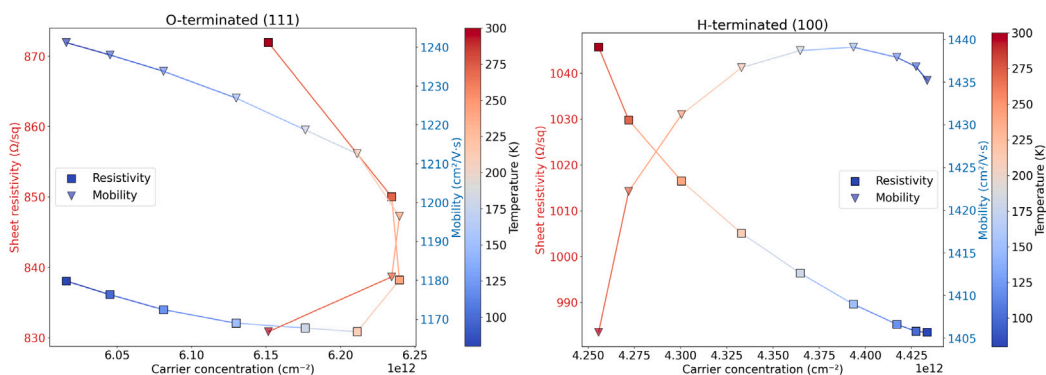


**Fig. 3.** Temperature dependence of sheet resistivity, carrier concentration, and Hall mobility for O-terminated (111), and H-terminated (100) before annealing from 80 to 300 K.

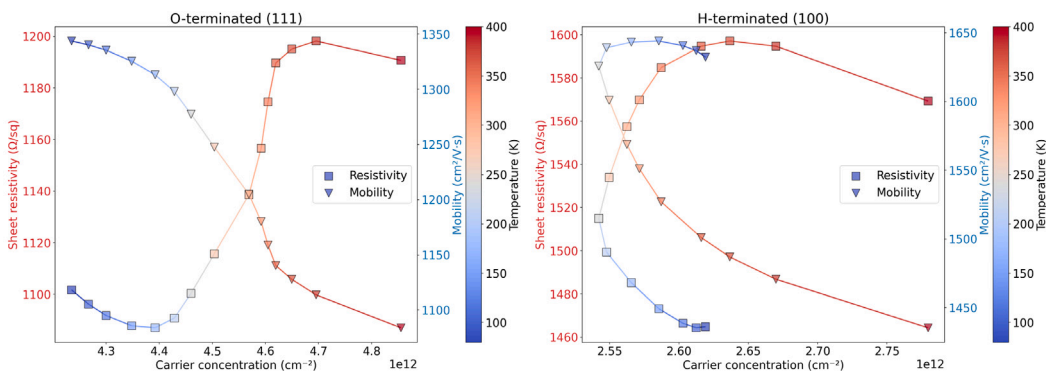


**Fig. 4.** Temperature dependence of sheet resistivity, carrier concentration, and mobility for O-terminated (111) and H-terminated (100) after annealing at 400 K for 30 min in vacuum, measured from 400 to 80 K.

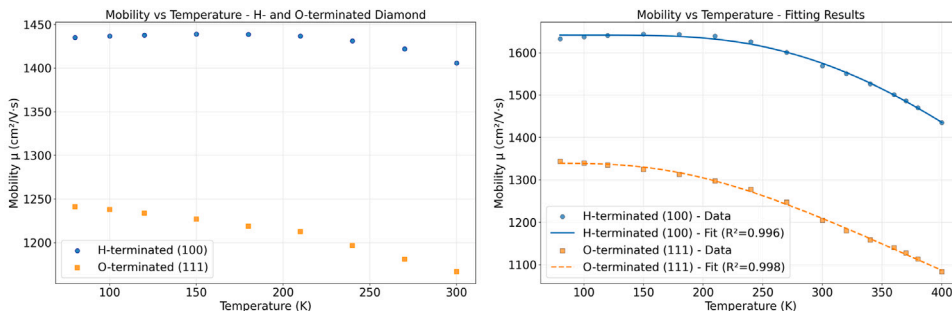


**Fig. 5.** Temperature dependence of the Hall mobility for H-terminated (100) and O-terminated (111) samples, before (left) and after annealing (right).

### CRediT authorship contribution statement

**Aisuloo Aitkulova:** Writing – review & editing, Writing – original draft, Visualization, Investigation, Formal analysis, Data curation, Conceptualization. **Markus Gabrysch:** Writing – review & editing, Software, Conceptualization. **Saman Majdi:** Writing – review & editing, Funding acquisition. **Nattakarn Suntornwipat:** Writing – review & editing. **Jan Isberg:** Writing – review & editing, Writing – original draft, Supervision, Project administration, Investigation, Funding acquisition, Conceptualization.

### Declaration of competing interest

The authors declare that they have no known competing financial interests or personal relationships that could have appeared to influence the work reported in this paper.

### Acknowledgments

The authors wish to acknowledge the Swedish Research Council (grant no. 2022-04186), the Carl Tryggers Foundation (grant nos. 22:2017 & 24:3542), and the Swedish Energy Agency, Sweden (grant no. P2019-90157) for financial support.

The Inorganic Chemistry group at Uppsala University is also acknowledged for providing access to furnaces, with special thanks to Pedro Berastigui for technical support.

### Data availability

Data will be made available on request.

## References

- [1] R. Katsumi, K. Takada, F. Jelezko, T. Yatsui, Recent progress in hybrid diamond photonics for quantum information processing and sensing, *Commun. Eng.* 4 (1) (2025) 85, <http://dx.doi.org/10.1038/s44172-025-00398-2>.
- [2] Z. Yan, W. Tong, X. Wang, D. Fan, A review of diamond composites for heat spreaders, *Compos. Part A: Appl. Sci. Manuf.* (2025) 109008, <http://dx.doi.org/10.1016/j.compositesa.2025.109008>.
- [3] J. Isberg, J. Hammersberg, E. Johansson, T. Wikstrom, D.J. Twitchen, A.J. Whitehead, S.E. Coe, G.A. Scarsbrook, High carrier mobility in single-crystal plasma-deposited diamond, *Science* 297 (5587) (2002) 1670–1672, <http://dx.doi.org/10.1126/science.1074374>.
- [4] B. Lyu, J. Chen, S. Wang, S. Lou, P. Shen, J. Xie, L. Qiu, I. Mitchell, C. Li, C. Hu, et al., Graphene nanoribbons grown in hBN stacks for high-performance electronics, *Nature* 628 (8009) (2024) 758–764, <http://dx.doi.org/10.1038/s41586-024-07243-0>.
- [5] O. Kovalchuk, S. Gong, H. Moon, Y.-W. Song, Graphene-advanced functional devices for integrated photonic platforms, *Npj Nanophotonics* 2 (1) (2025) 31, <http://dx.doi.org/10.1038/s44310-025-00072-7>.
- [6] G. Zhang, Q. Luo, J. Yao, S. Zhong, H. Wang, F. Xue, B. Yu, K.P. Loh, Y. Zhang, All-in-one neuromorphic hardware with 2D material technology: current status and future perspective, *Chem. Soc. Rev.* (2025) <http://dx.doi.org/10.1039/D5CS00251F>.
- [7] M.A. Ahmed, M.S. Saagoto, F. Mahbub, P. Barua, Graphene for qubits: A brief review, in: X.-S. Yang, S. Sherratt, N. Dey, A. Joshi (Eds.), *Proceedings of Tenth International Congress on Information and Communication Technology*, Springer Nature Singapore, Singapore, 2025, pp. 193–201, [http://dx.doi.org/10.1007/978-981-96-6435-1\\_15](http://dx.doi.org/10.1007/978-981-96-6435-1_15).
- [8] M. Brzhezinskaya, O. Kononenko, V. Matveev, A. Zotov, I.I. Khodos, V. Levashov, V. Volkov, S.I. Bozhko, S.V. Chekmazov, D. Roshchupkin, Engineering of numerous moiré superlattices in twisted multilayer graphene for twistrionics and straintronics applications, *ACS Nano*. 15 (7) (2021) 12358–12366, <http://dx.doi.org/10.1021/acsnano.1c04286>.
- [9] O. Kononenko, M. Brzhezinskaya, A. Zotov, V. Korepanov, V. Levashov, V. Matveev, D. Roshchupkin, Influence of numerous moiré superlattices on transport properties of twisted multilayer graphene, *Carbon* 194 (2022) 52–61, <http://dx.doi.org/10.1016/j.carbon.2022.03.033>.
- [10] M.C. Lemme, D. Akinwande, C. Huyghebaert, C. Stampfer, 2D materials for future heterogeneous electronics, *Nat. Commun.* 13 (1) (2022) 1392, <http://dx.doi.org/10.1038/s41467-022-29001-4>.
- [11] P. Bøggild, Research on scalable graphene faces a reproducibility gap, *Nat. Commun.* 14 (1) (2023) 1126, <http://dx.doi.org/10.1038/s41467-023-36891-5>.
- [12] K. Watanabe, N. Miura, H. Taguchi, T. Komatsu, A. Aratake, T. Makita, M. Tanabe, T. Wakimoto, S. Kumagai, T. Okamoto, et al., All-carbon-based complementary integrated circuits, *Adv. Mater. Technol.* 9 (5) (2024) 2301673, <http://dx.doi.org/10.1002/admt.202301673>.
- [13] D. Belotckovtceva, G. Datt, H. Nameirakpam, A. Aitkulova, N. Suntornwipat, S. Majdi, J. Isberg, M.V. Kamalakar, Extreme current density and breakdown mechanism in graphene on diamond substrate, *Carbon* 237 (2025) 120108, <http://dx.doi.org/10.1016/j.carbon.2025.120108>.
- [14] M. Asad, S. Majdi, A. Vorobiev, K. Jeppson, J. Isberg, J. Stake, Graphene FET on diamond for high-frequency electronics, *IEEE Electron Device Lett.* 43 (2) (2021) 300–303, <http://dx.doi.org/10.1109/LED.2021.3139139>.
- [15] A. Aitkulova, S. Majdi, N. Suntornwipat, J. Isberg, Graphene on single-crystal diamond for electronic applications: A brief review, *Phys. Status Solidi (A)* 222 (5) (2025) 2400567, <http://dx.doi.org/10.1002/pssa.202400567>.
- [16] Z.-C. Ma, N. Gao, S.-H. Cheng, J.-S. Liu, M.-C. Yang, P. Wang, Z.-Y. Feng, Q.-L. Wang, H.-D. Li, Wettability and surface energy of hydrogen-and oxygen-terminated diamond films, *Chin. Phys. Lett.* 37 (4) (2020) 046801, <http://dx.doi.org/10.1088/0256-307X/37/4/046801>.
- [17] A.F. Abdelaal, T. Laoui, A. Ibrahim, B. Salhi, M.R. Akhter, Interplay of surface hydrophilicity and graphene transfer on SiO<sub>2</sub>/Si substrate: Implications for electrical conductivity and optical transparency, *Int. J. Adhesion Adhesives* 140 (2025) 104009, <http://dx.doi.org/10.1016/j.ijadhadh.2025.104009>.
- [18] J. Fuhrmann, J. Lang, J. Scharpf, N. Striegler, T. Unden, P. Neumann, J. Bansmann, F. Jelezko, Probing coherence properties of shallow implanted NV ensembles under different oxygen terminations, *Mater. Quantum Technol.* 4 (4) (2024) 041001, <http://dx.doi.org/10.1088/2633-4356/ad9376>.
- [19] A. Chemin, M.K. Kuntumalla, M. Brzhezinskaya, T. Petit, A. Hoffman, Depth profiling of microwave nitrogen-terminated polycrystalline diamond surfaces by energy-dependent X-ray photoelectron spectroscopy, *Appl. Surf. Sci.* 661 (2024) 160082, <http://dx.doi.org/10.1016/j.apsusc.2024.160082>.
- [20] M.K. Kuntumalla, A. Chemin, N.M. Doron, M. Brzhezinskaya, T. Petit, A. Hoffman, Impact of acid etching on surfaces and near-surface region in nitrogen plasma terminated polycrystalline diamond, *Diam. Relat. Mater.* 158 (2025) 112623, <http://dx.doi.org/10.1016/j.diamond.2025.112623>.
- [21] M. Yang, Q. Yuan, M. Qiu, Z. Jia, G. Yang, K. Nishimura, C.-T. Lin, X. Sun, N. Jiang, Y. Hu, Temperature dependence of two-dimensional hole gas on hydrogen-terminated diamond surface, *Diam. Relat. Mater.* 139 (2023) 110414, <http://dx.doi.org/10.1016/j.diamond.2023.110414>.
- [22] K.J. Brown, E. Chartier, E.M. Sweet, D.A. Hopper, L.C. Bassett, Cleaning diamond surfaces using boiling acid treatment in a standard laboratory chemical hood, *J. Chem. Health Saf.* 26 (6) (2019) 40–44, <http://dx.doi.org/10.1016/j.jchas.2019.06.001>.
- [23] W. Kern, The evolution of silicon wafer cleaning technology, *J. Electrochem. Soc.* 137 (6) (1990) 1887, <http://dx.doi.org/10.1149/1.2086825>.
- [24] K.I. Bolotin, K.J. Sikes, J. Hone, H. Stormer, P. Kim, Temperature-dependent transport in suspended graphene, *Phys. Rev. Lett.* 101 (9) (2008) 096802, <http://dx.doi.org/10.1103/PhysRevLett.101.096802>.
- [25] L. Wang, I. Meric, P. Huang, Q. Gao, Y. Gao, H. Tran, T. Taniguchi, K. Watanabe, L. Campos, D. Muller, et al., One-dimensional electrical contact to a two-dimensional material, *Science* 342 (6158) (2013) 614–617, <http://dx.doi.org/10.1126/science.1244358>.
- [26] S. Park, M.A. Shehzad, M.F. Khan, G. Nazir, J. Eom, H. Noh, Y. Seo, Effect of grain boundaries on electrical properties of polycrystalline graphene, *Carbon* 112 (2017) 142–148, <http://dx.doi.org/10.1016/j.carbon.2016.11.010>.
- [27] W. Hu, Z. Li, J. Yang, Diamond as an inert substrate of graphene, *J. Chem. Phys.* 138 (5) (2013) <http://dx.doi.org/10.1063/1.4789420>.
- [28] J.-H. Chen, C. Jang, S. Xiao, M. Ishigami, M.S. Fuhrer, Intrinsic and extrinsic performance limits of graphene devices on SiO<sub>2</sub>, *Nature Nanotechnology* 3 (4) (2008) 206–209, <http://dx.doi.org/10.1038/nnano.2008.58>.
- [29] S. Majdi, V. Djurberg, M. Asad, A. Aitkulova, N. Suntornwipat, J. Stake, J. Isberg, Enhanced hall mobility in graphene-on-electronic-grade diamond, *Appl. Phys. Lett.* 123 (1) (2023) <http://dx.doi.org/10.1063/5.0156108>.
- [30] S. Tanabe, Y. Sekine, H. Kageshima, M. Nagase, H. Hibino, Carrier transport mechanism in graphene on SiC (0001), *Phys. Rev. Condens. Matter Mater. Phys.* 84 (11) (2011) 115458, <http://dx.doi.org/10.1103/PhysRevB.84.115458>.